NASA Technical Memorandum 84319

Unsteady Laminar Boundary-Layer Calculations on Oscillating Configurations Including Backflow

Part I: Flat Plate, Oscillating in its Own Plane

W. Geissler

March 1983

NASA
National Aeronautics and
Space Administration

Unsteady Laminar Boundary-Layer Calculations on Oscillating Configurations Including Backflow
Part I: Flat Plate, Oscillating in its Own Plane

W. Geissler, Ames Research Center, Moffett Field, California

Page intentionally left blank

TABLE OF CONTENTS

Page intentionally left blank

LIST OF SYMBOLS

f	frequency
ℓ	reference length
ℓ, m, n	indices of mesh points in x-, T-, y-directions
p	pressure
$Re = \dfrac{U_\infty \ell}{\nu}$	Reynolds number
$T = \dfrac{t U_\infty}{\ell}$	dimensionless time, $\bar{T} = \dfrac{T}{2\pi/\omega^*}$
t	time
U(t)	outer flow velocity (with reference to U_∞)
U_∞	reference velocity
u(x,t), v(x,t)	x-, y-velocity components within the boundary layer (with reference to U_∞)
$\bar{v} = v\sqrt{Re}$	transformed normal velocity
x	coordinate in flow direction
y	coordinate normal to the plate
'	derivation with respect to η
$\eta = y\sqrt{Re}$	transformed normal coordinate
ε	oscillation amplitude
$\xi = i\omega^* \cdot x$	unsteady parameter
ν	kinematic viscosity
$\omega^* = \dfrac{2\pi f \ell}{U_\infty}$	reduced frequency

UNSTEADY LAMINAR BOUNDARY LAYER CALCULATIONS ON OSCILLATING

CONFIGURATIONS INCLUDING BACKFLOW

PART I: FLAT PLATE, OSCILLATING IN ITS OWN PLANE

W. Geissler*

Ames Research Center

SUMMARY

A finite difference method has been developed to calculate the unsteady boundary layer over an oscillating flat plate. Low- and high-frequency approximations were used for comparison with numerical results. Special emphasis was placed on the behavior of the flow and on the numerical calculation procedure as soon as reversed flow has occurred over part of the oscillation cycle. The numerical method displayed neither problems nor singular behavior at the beginning of or within the reversed flow region. Calculations, however, came to a limit where the back-flow region reached the plate's leading edge in the case of high oscillation amplitudes. It is assumed that this limit is caused by the special behavior of the flow at the plate's leading edge where the boundary layer equations are not valid.

INTRODUCTION

Unsteady viscous flows play a dominant role in several fields of aeronautical applications and have severe influences on lift and drag characteristics, particularly in cases where flow separation occurs. Dynamic-stall investigations on oscillating 3-D rotor-blade tips (ref. 1) and active control investigations on a supercritical wing section with an oscillating, trailing-edge control (ref. 2) are two of these cases in which unsteady separated flows are dominant. These two cases have been investigated recently by using intensive wind-tunnel measurements made in the Deutsche Forschungs- und Versuchsanstalt für Luft- und Raumfahrt (DFVLR) Göttingen. Both cases have been compared with inviscid-panel-method calculations (refs. 1, 3) to illustrate the influence of viscosity and its effects on the steady and unsteady airloads under nonseparated and separated flow conditions. These studies indicated that the influence of viscosity in nonseparated flow is created mainly by boundary layer displacement effects. These effects can easily be taken into account in theoretical calculations by adding the displacement thickness to the wing profile and then calculating pressures and forces on the modified configuration.

Under unsteady separated flow conditions, however, this procedure is not applicable. Comparisons between inviscid theory and experiments in this case have shown that special characteristic features of the pressure distributions occur in most of the investigated cases. These features can be described by strong phase shifts within the first-harmonic unsteady pressure distributions when they are compared to

---

*NRC, Deutsche Forschungs- und Versuchsanstalt für Luft- und Raumfahrt Forschungsbereich Werkstoffe und Bauweisen.

inviscid calculations. These phase shifts may lead to a shift of the real-part pressure peak (at the hinge line of a wing having oscillating control) into the imaginary part, exerting a strong influence on the applicability of wing-control systems for active-control purposes.

To investigate these viscous phenomena, unsteady boundary-layer calculations have been performed which include flow regimes in which back-flow occurs along the oscillating wall. The present study includes the case of a semi-infinite flat plate, oscillating in its own plane. This problem has been treated in several investigations from the first studies by Lighthill (ref. 4), who calculated approximate high- and low-frequency solutions to the more sophisticated numerical procedures of Phillips and Ackerberg (ref. 5), which deal with regions of backflow. McCroskey and Phillippe (ref. 6) extended their method to the dynamic stall problem of oscillating profiles which include laminar and turbulent unsteady boundary layer calculations. The present study of an oscillating flat plate is assumed to be a necessary step in checking the validity and applicability of the numerical method which will be applied to the more complicated case of oscillating profiles. Some interesting features have been found in the flat plate boundary layer studies which may give an indication of the behavior of more complicated unsteady viscous flows.

UNSTEADY BOUNDARY LAYER EQUATIONS

Unsteady, viscous-incompressible flow in the vicinity of an oscillating wall is governed by the well-known set of unsteady boundary layer equations expressing the conservation of mass and momentum (ref. 7):

$$\frac{\partial u}{\partial x} + \frac{\partial \bar{v}}{\partial \eta} = 0 \tag{1}$$

$$\frac{\partial u}{\partial T} + u \frac{\partial u}{\partial x} + \bar{v} \frac{\partial u}{\partial \eta} = - \frac{\partial p}{\partial x} + \frac{\partial^2 u}{\partial \eta^2} \tag{2}$$

with $-(\partial p/\partial x) = (\partial U/\partial T)$ in the flat plate case.

In equations (1) and (2), the different quantities have been made dimensionless, and the normal coordinate and the normal velocity have been multiplied by $\sqrt{Re}$. The boundary conditions for the system of equations read:

$$u = \bar{v} = 0 \quad \text{for} \quad \eta = 0$$

$$u = U \quad \text{for} \quad \eta = \infty$$

In the flat plate case, the velocity at the outer edge of the boundary layer is assumed to be given by

$$U(T) = U_\infty (1 + \varepsilon \cdot e^{i\omega^* T}) \tag{3}$$

with ε as the oscillation amplitude. Three different solution procedures will be developed to include:

2

1. A low-frequency approximation, where the unsteady parameter $\xi = x \cdot \omega^* < 1$;

2. A high-frequency approximation, where the unsteady parameter $\xi \gg 1$;

3. A finite-difference procedure which numerically calculates the unsteady boundary layer for arbitrary values of ξ.

Comparisons between the low- /high-frequency approximations and the numerical results will provide an excellent check of the validity of the numerical procedure.

LOW-FREQUENCY APPROXIMATION

In the boundary layer equations (1) and (2), only the steady and first harmonic terms are retained. The stream-wise velocity component is defined by

$$u = f'(\eta) + \varepsilon \Phi'(\xi,\eta) e^{i\omega^*T} \tag{4}$$

As long as $\xi < 1$, a power-series expansion in ξ can be applied for Φ:

$$\Phi(\xi,\eta) = \sum_{k=0}^{\infty} \xi^k \phi_k(\eta) e^{i\omega^*T} \tag{5}$$

leading to

$$u = f'(\eta) + \varepsilon \sum_{k=0}^{\infty} \xi^k \phi_k'(\eta) e^{i\omega^*T} \tag{6}$$

with f as the well-known Blasius function. With a properly chosen normal velocity component

$$v = \frac{1}{2}\sqrt{\frac{U_\infty}{x}}\left\{(\eta f' - f) + \varepsilon\left(\eta \sum_{k=0}^{\infty} \xi^k \phi_k' - \sum_{k=0}^{\infty} \xi^k \phi_k\right) e^{i\omega^*T} - 2\varepsilon\xi \sum_{k=1}^{\infty} k\xi^{k-1}\phi_k \, e^{i\omega^*T}\right\} \tag{7}$$

the continuity equation (1) is automatically fulfilled.

The following system of equations is obtained by combining expressions (6) and (7) and the corresponding derivatives with equation (3) in the momentum equation (2):

3

Equation	Boundary condition

$$f \cdot f'' + 2f''' = 0$$

(Blasius equation)

$$\frac{1}{2} f\phi_0'' + \frac{1}{2} f''\phi_0 + \phi_0'''$$

(quasi-steady)

$$1 - \phi_0' - f'\phi_1' + \frac{1}{2} f\phi_1''$$

$$+ \frac{3}{2} f''\phi_1 + \phi_1'''$$

(linear)

$$- \phi_{n-1}' - nf'\phi_n' + \frac{1}{2} f\phi_n''$$

$$+ \left(n + \frac{1}{2}\right) f''\phi_n + \phi_n'''$$

(quadratic and higher)

Boundary conditions:

$f = f' = 0$ for $\eta = 0$
$f' = 1$ for $\eta = \infty$

$\phi_0 = \phi_0' = 0$ for $\eta = 0$
$\phi_0' = 1$ for $\eta = \infty$

$\phi_1 = \phi_1' = 0$ for $\eta = 0$
$\phi_1' = 0$ for $\eta = \infty$

$\phi_n = \phi_n' = 0$ for $\eta = 0$
$\phi_n' = 0$ for $\eta = \infty$

$$\tag{8}$$

The system of equations (8) is solved sequentially, starting with the Blasius equation and then solving the quasi-steady, linear, and higher-order equations by taking the solutions of the previous steps into account.

The numerical solution of the system of ordinary differential equations (8) is carried out by a fourth-order Runge-Kutta integration procedure which has been used for calculating steady, 3-D stagnation-point flows (refs. 8, 9). Typical results are plotted in figure 1, which gives the real and imaginary parts of the function Φ (eq. (5)) versus η for various parameters ξ. For each of these calculations, the series expansion in equation (5) was represented up to the 11th member. The quasi-steady curve in figure 1 (broken line) is the limiting case of $k = 0$ in equation (5), which indicates that the function Φ is independent of ξ and therefore is independent of ω^*. The overshoot at the outer boundary condition, which increases with increasing ξ, is typical behavior of the real parts of Φ. Further results of the low-frequency approximation are compared directly with the numerical results.

HIGH-FREQUENCY APPROXIMATION

In the high-frequency case, a procedure similar to that used for low frequencies is not straightforward. A representation of Φ by a series expansion of $1/\xi$, for instance, does not lead to the correct approximation of the governing equations. Therefore, a different procedure is followed here.

By using equation (4) for u and using equation (7) for v without taking into account the series expansion of Φ, the following well-known differential equation for Φ (ref. 7, p. 434) is derived

$$\Phi''' + \frac{1}{2} f\Phi'' - \xi\Phi' + \frac{1}{2} f''\Phi - f'\xi\Phi_\xi' + f''\xi\Phi_\xi + \xi = 0 \tag{9}$$

This equation holds for arbitrary values of ξ. Equation (9) cannot be solved directly because of the unknown ξ-derivatives. To obtain approximate values for

Φ_ξ and $\Phi_\xi^!$, an approximate form of equation (9) is used in which only the terms involving ξ and the derivative of the highest order are retained (in accordance with the theory of differential equations with large parameters) (ref. 4):

$$\Phi''' - \xi\Phi' + \xi = 0 \tag{10}$$

for which an analytical solution exists (ref. 4):

$$\Phi'(\xi,\eta) = 1 - e^{-\sqrt{\xi}\cdot\eta} \tag{11}$$

$$\Phi(\xi,\eta) = \eta + \frac{1}{\sqrt{\xi}} e^{-\sqrt{\xi}\cdot\eta} \tag{12}$$

The derivatives of equations (11) and (12) with respect to ξ are

$$\Phi_\xi' = \frac{1}{2\sqrt{\xi}} e^{-\sqrt{\xi}\cdot\eta} \tag{13}$$

and

$$\Phi_\xi = -\frac{1}{2\sqrt{\xi}} e^{-\sqrt{\xi}\cdot\eta} \left(\frac{1}{\xi} + \frac{\eta}{\sqrt{\xi}}\right) \tag{14}$$

The derivatives from equations (13) and (14) are now inserted into equation (8), which can then be solved by using the same numerical technique applied for the solution of each equation of system (8). The results are assumed to be valid not only for extremely high values, but also for moderately high values of ξ. Results of these calculations will also be discussed in direct comparison with the corresponding numerical results of the finite-difference procedure.

NUMERICAL CALCULATION PROCEDURE

The numerical procedure follows the ideas of Hall (ref. 10), who developed a method to solve the unsteady 2-D boundary layers for a flat plate impulsively set into motion. For the present case of harmonic oscillations, the time parameter, T, is first referred to the wavelength of the harmonic oscillation

$$\bar{T} = \frac{T}{2\pi/\omega^*} \tag{15}$$

which changes equation (2) into

$$\frac{\partial u}{\partial \bar{T}} \frac{\omega^*}{2\pi} + u \frac{\partial u}{\partial x} + \bar{v} \frac{\partial u}{\partial \eta} = \frac{\partial U}{\partial \bar{T}} \frac{\omega^*}{2\pi} + \frac{\partial^2 u}{\partial \eta^2} \tag{16}$$

For discretization of equations (1) and (16), a Crank-Nicolson type of scheme is used (fig. 2): information at points ①, ②, and ③ is assumed to be given, and new values are calculated at position ④.

5

This method is implicit in the direction normal to the wall (η-direction, index n) and explicit in the two flow directions ($\overline{T}$, index m and x, index ℓ).

For central differentiation about point ⑤ in figure 2, the following expressions are derived with the abbreviations:

$$u_n^s = \frac{1}{4} \left(u_{\ell+1,m,n} + u_{\ell,m+1,n} + u_{\ell,m,n}\right)$$

$$u_n^\ell = u_{\ell+1,m,n} - u_{\ell,m+1,n} - u_{\ell,m,n} \tag{17}$$

$$u_n^m = u_{\ell,m+1,n} - u_{\ell+1,m,n} - u_{\ell,m,n}$$

The velocities and their derivatives at midpoint ⑤ are

$$\left.\begin{aligned}
u_{\ell+(1/2),n+(1/2),n} &= \frac{1}{4} u_{\ell+1,m+1,n} + u_n^s \\[6pt]
\left(\frac{\partial u}{\partial x}\right)_{\ell+(1/2),m+(1/2),n} &= \frac{1}{2\Delta x} \left(u_{\ell+1,m+1,n} + u_n^\ell\right) \\[6pt]
\left(\frac{\partial u}{\partial \eta}\right)_{\ell+(1/2),m+(1/2),n} &= \frac{1}{2\Delta\eta} \left(\frac{1}{4} u_{\ell+1,m+1,n+1} - \frac{1}{4} u_{\ell+1,m+1,n-1} + u_{n+1}^s - u_{n-1}^s\right) \\[6pt]
\left(\frac{\partial^2 u}{\partial \eta^2}\right)_{\ell+(1/2),m+(1/2),n} &= \frac{1}{\Delta\eta^2} \left(\frac{1}{4} u_{\ell+1,m+1,n+1} - \frac{1}{2} u_{\ell+1,m+1,n} + \frac{1}{4} u_{\ell+1,m+1,n-1} \right.\\[6pt]
&\qquad \left. + u_{n+1}^s - 2u_n^s + u_{n-1}^s\right) \\[6pt]
\left(\frac{\partial u}{\partial \overline{T}}\right)_{\ell+(1/2),m+(1/2),n} &= \frac{1}{2\Delta\overline{T}} \left(u_{\ell+1,m+1,n} + u_n^m\right)
\end{aligned}\right\} \tag{18}$$

The introduction of the various terms of equation (18) into the momentum equation (16) yields

$$a_n u_{\ell+1,m+1,n+1} + b_n u_{\ell+1,m+1,n} + c_n u_{\ell+1,m+1,n-1} = d_n \tag{19}$$

with the coefficients

$$\left.\begin{aligned}
a_n &= \frac{1}{8\Delta\eta} v_{\ell+(1/2),m+(1/2),n} - \frac{1}{4\Delta\eta^2} \\[6pt]
b_n &= \frac{\kappa}{2\Delta\overline{T}} + \frac{1}{4\Delta x} u_{\ell+1,m,n} + \frac{1}{2\Delta\eta^2} \\[6pt]
c_n &= \frac{1}{8\Delta\eta} v_{\ell+(1/2),m+(1/2),n} - \frac{1}{4\Delta\eta^2}
\end{aligned}\right\} \tag{20}$$

6

$$d_n = -\frac{\kappa}{2\Delta\bar{T}} u_n^m - \frac{1}{8\Delta x} u_{\ell+1,m+1,n}^2 - \frac{1}{2\Delta x} u_n^s u_n^\ell - \frac{1}{2\Delta\eta} v_{\ell+(1/2),m+(1/2),n} (u_{n+1}^s - u_{n-1}^s)$$

$$+ \frac{\kappa}{2\Delta\bar{T}} (U_{\ell+1,m+1} + U^m) + \frac{1}{2\Delta x} \left(\frac{1}{4} U_{\ell+1,m+1} + U^s\right)(U_{\ell+1,m+1} + U^\ell)$$

$$+ \frac{1}{\Delta\eta^2} (u_{n+1}^s - 2u_n^s + u_{n-1}^s)$$

$$\left.\begin{array}{r}(20)\\(\text{cont})\end{array}\right.$$

and with $\kappa = \omega^*/2\pi$.

For the continuity equation, the following expressions are derived:

$$\left(\frac{\partial u}{\partial x}\right)_{\ell+(1/2),m+(1/2),n+(1/2)} = \frac{1}{2} \left[\left(\frac{\partial u}{\partial x}\right)_{\ell+(1/2),m+(1/2),n+1} + \left(\frac{\partial u}{\partial x}\right)_{\ell+(1/2),m+(1/2),n}\right]$$

$$\left(\frac{\partial v}{\partial\eta}\right)_{\ell+(1/2),m+(1/2),n+(1/2)} = \frac{1}{\Delta\eta} [v_{\ell+(1/2),m+(1/2),n+1} - v_{\ell+(1/2),m+(1/2),n}]$$

$$v_{\ell+(1/2),m+(1/2),n+1} = v_{\ell+(1/2),m+(1/2),n} - \frac{\Delta\eta}{4\Delta x} [u_{\ell+1,m+1,n+1}$$

$$+ u_{\ell+1,m+1,n} + u_{n+1}^\ell + u_n^\ell]$$

$$(21)$$

To start the numerical calculation, simple, linearly extrapolated values from the positions ①, ②, and ③ are determined in position ④. Equation (21) is first calculated for the normal velocity component through the boundary layer. With these initial estimates for v, equation (19) combined with the coefficients from equation (20) can be calculated by means of the solution of a linear system of equations with a tridiagonal coefficient matrix (ref. 8).

The newly calculated $u_{\ell+1,m+1,n}$ values then enter equation (21), thus starting a second cycle of the iterative procedure. This process is repeated until the differences in the velocity components, u, between two cycles are less than a given small number. Calculation then continues in the next grid point.

The calculation first progresses in the x-direction (index ℓ) until the maximum x-value is reached and then continues one step, $\Delta\bar{T}$, in the time direction (index m), etc. For the grid points (ℓ, 1) at $\bar{T}$ = 0, the Blasius profiles, f', are used as initial values. At the grid points (1, m) at x = Δx, the solution of equation (8) is used as initial values along the time axis.

Calculations were continued up to the third cycle, although the differences between the second and third cycle turned out to be negligibly small in most cases.

7

DISCUSSION OF THE RESULTS

A series of calculations have been performed to test the validity and effectiveness of the numerical procedure. Comparisons with the corresponding low- and high-frequency solutions were made to investigate the accuracy of the results.

Figures 3 and 4 show, first, wall shear-stress (τ_w) and boundary-layer-displacement thickness (δ_1) over a period of time with $\xi = x \cdot \omega^*$ (x = the coordinate from the plate's leading edge) as a parameter. The numerical results for the first and second periods are compared with the low-frequency approximation. The amplitude of oscillation is $\varepsilon = 0.2$. Except for some minor deviations at x = 0.1, agreement between both results is very good. Both τ_w- and δ_1-distributions show the well-known phase lead with increasing value of ξ $(= x\omega^*)$, which tends to 45° for τ_w and gives a maximum value for δ_1 up to approximately 20°. Figures 5 and 6 show corresponding results for τ_w and δ_1 plotted versus ξ for various dimensionless time levels. The differences between the first and second period of the numerical calculation decrease as time increases. Again, agreement between numerical results and the low-frequency solution is very good.

Figures 7 and 8 show corresponding results for the higher-frequency case $\omega^* = 5$. In figure 7 at approximately x = 0.6 $(\xi = 3)$ the wall shear stress has negative values over part of the cycle. The region of negative τ, that is, the back-flow region, increases as x increases. The numerical calculation method proceeds through these reversed-flow regions without any numerical problems. For the largest x-values (x = 0.9), the results of the high-frequency approximation are discussed. Only minor differences in both cases are seen for τ_w and for δ_1. In figure 8 (δ_1) results are plotted for the first three periods of oscillation. The number of cycles must be increased as the distance from the plate's leading edge increases to reach the steady, periodic solution. At $\xi = 4.5$ as many as four cycles must be calculated until a good fit with the high-frequency results is obtained.

Numerical calculation has been continued in the x-direction as far as x = 2.5, corresponding to a frequency parameter of $\xi = 12.5$. The calculation ran without any complications, although the back-flow region was extended to $0.4 < \bar{T} < 0.8$. However, with increasing back-flow velocities, the numerical calculation had an increased tendency to oscillate. These oscillations could easily be avoided by applying a simple, linear-interpolation procedure over three mesh points in the x-direction, which has already been applied successfully for calculation of 3-D steady boundary layers (refs. 8, 9).

There should be no problems for linear stability in cases in which the mesh sizes in the x- and $\bar{T}$-directions are equal. The Courant-Friedrich-Levy (CFL) condition leads to the limit

$$|\Delta x| > |\min(u_{\ell+1,m,n})\Delta\bar{T}| \qquad (22)$$

with $\min(u_{\ell+1,m,n})$ as the largest negative u-velocity component within the back-flow region. It is obvious that for $\Delta x = \Delta\bar{T}$:

$$|\min(u_{\ell+1,m,n})| \leqq 1 \qquad (23)$$

The limit for equation (23) was by no means exceeded in the previously discussed cases.

8

Figures 9-12 show results for the high-frequency case ($\omega^* = 5$) with increased oscillation amplitude ε. It can be observed in the lower-amplitude case ($\varepsilon = 0.2$, fig. 8) that the time dependency of δ_1 deviates with an increasing value for x from a simple sinusoidal behavior: beyond the reversed-flow region the boundary layer steepens. This behavior of δ_1 is much more pronounced with increasing oscillation amplitude and can be studied in detail in figure 10. If a Fourier analysis of $\delta_1(T)$ is carried out, strong in-phase components of the second harmonic are obtained. The wall shear-stress curves (fig. 9), however, show only small deviations from a pure sinusoidal behavior.

Figure 11 shows details of the u-velocity components in the vicinity of the wall where considerable back flow occurs over part of the cycle. Correspondence between the numerical data and the high-frequency results are, again, extremely good. This agreement ensures that the numerical method is of sufficiently high accuracy and reliability.

To investigate the influences of increasing oscillation amplitude, ε was increased to values as large as 0.5, 0.7, and 0.9. Figures 12 and 13 show the corresponding high-frequency results for τ_w and δ_1. It is remarkable to see the increasing peak of δ_1 beyond the back-flow region in figure 13. At $\varepsilon = 0.9$ the peak value reaches 14.6, and at $\varepsilon = 1.0$ the calculation discloses a singularity at point $T = 0.75$. This singularity is caused by the definition of the displacement thickness which refers to the velocity at the outer edge of the boundary layer. This velocity tends to zero at a particular point of the cycle for the case of $\varepsilon = 1$. The wall shear-stress behavior (fig. 12) is regular as in the smaller ε-cases, without irregularities even at $\varepsilon = 1$.

The numerical-calculation procedure, however, was limited as soon as the reversed-flow region reached back to the leading edge of the plate during part of the cycle. This was the case for $\omega^* = 5$ at $\varepsilon = 0.5$ and $0.65 > x > 0.75$. The solution then started to oscillate with increasing amplitudes. There was no possibility of avoiding these oscillations by means of an interpolation procedure. It is assumed, however, that the breakdown of the numerical method is caused by difficulties at the leading edge of the plate, and not by the increasing, reversed-flow regions.

CONCLUSION

A numerical method has been developed to calculate the unsteady laminar boundary layer over an oscillating flat plate. This investigation was made to gain insight into flow behavior, and to establish the applicability of a numerical-calculation procedure which, based on the boundary-layer concept, could be applied as soon as flow reversal occurred over parts of the cycle. Corresponding low- and high-frequency solutions have been developed for comparison with the full numerical results. For both of these limiting cases, agreement with the numerical results were good. No numerical problems occurred within regions of reversed flow. The numerical calculation procedure, however, came to a limit as soon as the back-flow region reached the leading edge of the plate. It is assumed that in this case the boundary layer concept is violated because of the more complicated flow behavior at the plate's leading edge. The most remarkable behavior is shown by the boundary-layer displacement thickness over a cycle of oscillation. With increasing amplitude, δ_1 increases rapidly beyond the back-flow region. This behavior can be observed with the relatively simple high-frequency approximation discussed previously.

The numerical procedure developed for oscillating flat plates should permit the development of a similar method for using oscillating profiles to investigate unsteady separation at high incidences and at moderate to large oscillation amplitudes.

REFERENCES

1. Geissler, W.: Dynamic Stall Investigations on a Rectangular Blade Tip. DFVLR IB 232-82 J 04, 1982.

2. Triebstein, H.; Destynder, R.; and Hansen, H.: Investigation of the Unsteady Airloads on a Transport Aircraft Type Airfoil with Two Interchangeable Oscillating Trailing Edge Flaps, at Transonic Speed and High Reynolds Numbers. Proc. of 13th Congress of International Council of Aeronautical Sciences, ICAS Paper 82-5.2.1, Seattle, Wash, vol. I, 1982.

3. Geissler, W.: Investigation of Unsteady Airloads on Wings with Oscillating Control for Active Control Purposes. 52nd Meeting of AGARD Structures and Materials Panel, AGARD Report 699, Cesme/Turkey, 1981.

4. Lighthill, M. J.: The Response of Laminar Skin Friction and Heat Transfer to Fluctuations in the Stream Velocity. Proc. of the Royal Society Ser. A., vol. 224, 1954.

5. Phillips, J. H.; and Ackerberg, A. C.: A Numerical Method of Integrating the Unsteady Boundary-Layer Equations when there are Regions of Backflow. J. Fluid Mech., vol. 58, Part 3, 1973, pp. 561-579.

6. McCroskey, W. J.; and Philippe, J. J.: Unsteady Viscous Flows on Oscillating Airfoils. AIAA J., vol. 13, no. 1, Jan. 1975, pp. 71-79.

7. Schlichting, H.: Boundary-Layer Theory. Seventh ed., McGraw-Hill, 1979.

8. Geissler, W.: Berechnung der laminaren dreidimensionalen Grenzschicht an unsymmetrisch umströmten Rotationskörpern mittels Differenzenverfahren. DFVLR IB 251-73 A 19, 1973.

9. Geissler, W.: Three-Dimensional Laminar Boundary Layer over a Body of Revolution at Incidence and with Separation. AIAA J., vol. 12, no. 12, Dec. 1974, pp. 1743-1745.

10. Hall, M. G.: A Numerical Method for Calculating Unsteady Two-Dimensional Laminar Boundary Layers. Ing. Arch., vol. 38, 1969, pp. 97-106.
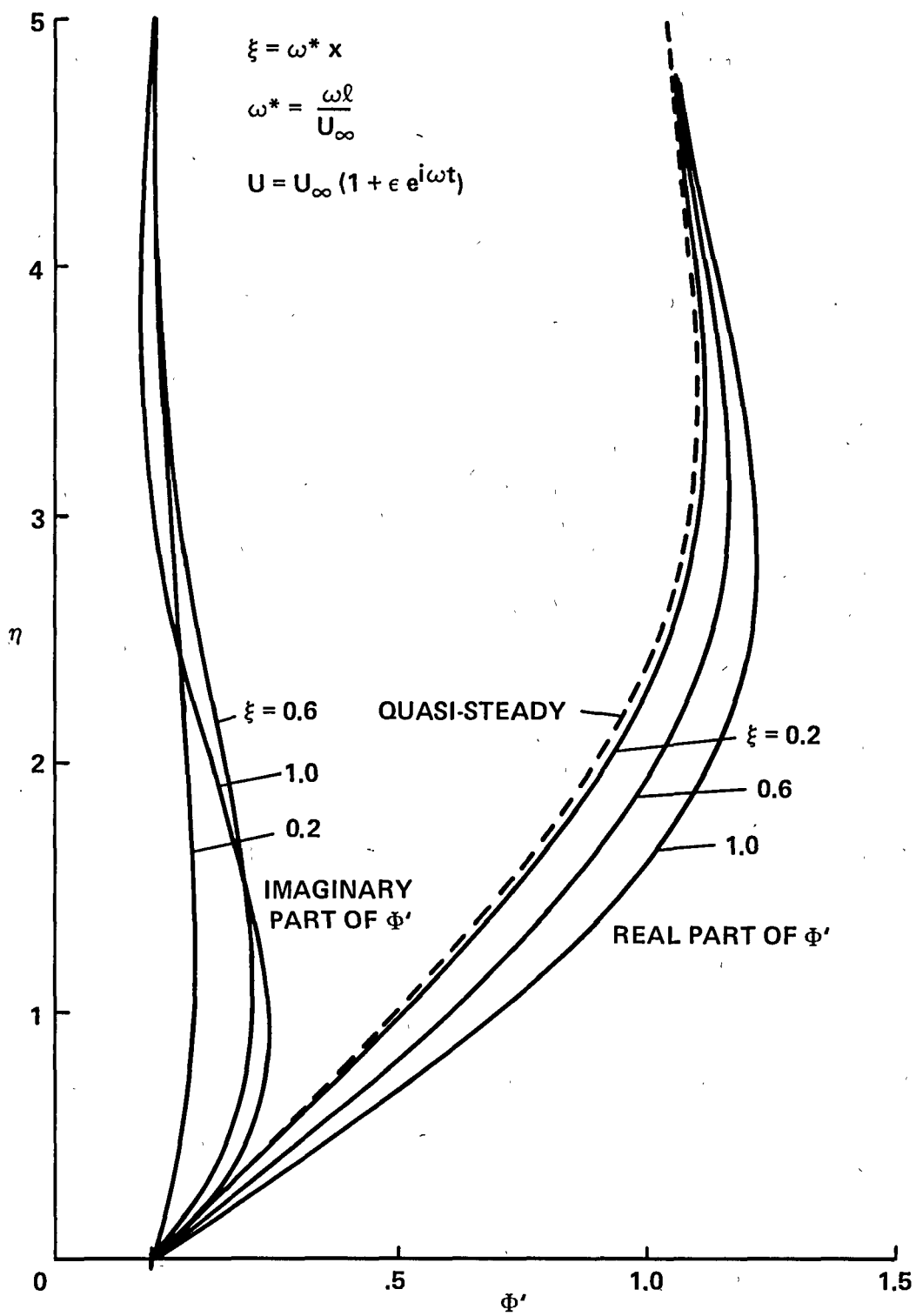
$$\xi = \omega^* x$$

$$\omega^* = \frac{\omega \ell}{U_\infty}$$

$$U = U_\infty (1 + \epsilon \, e^{i\omega t})$$

Figure 1.- Low-frequency solution: real and imaginary boundary layer profiles.
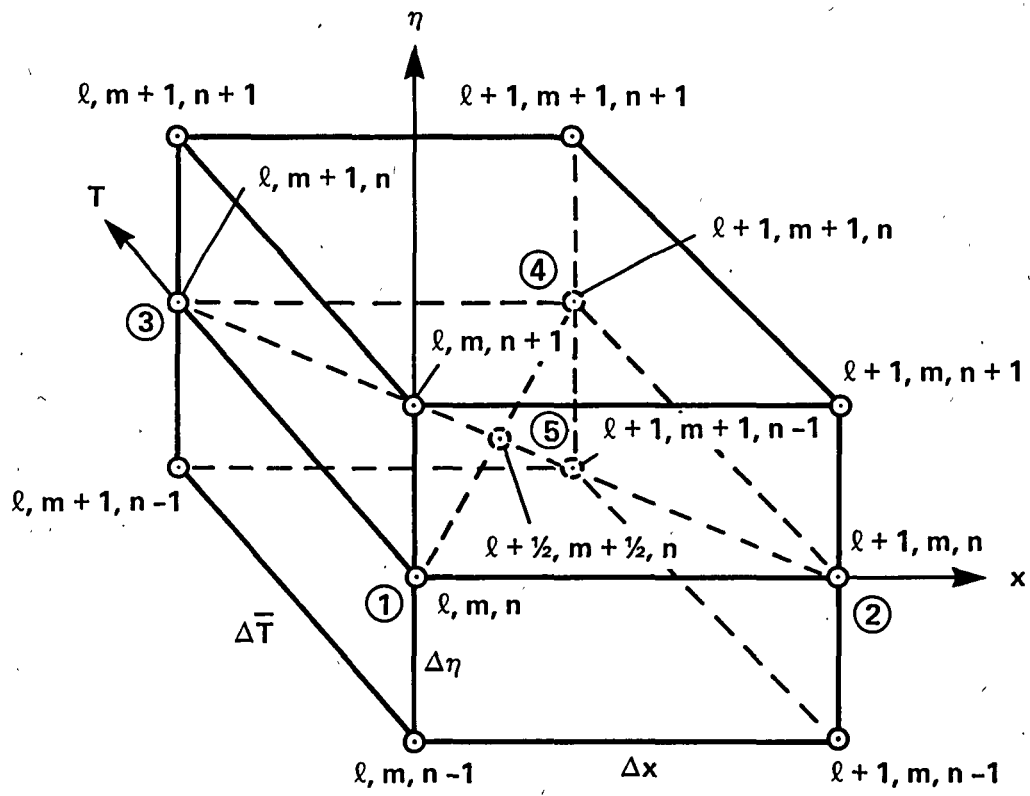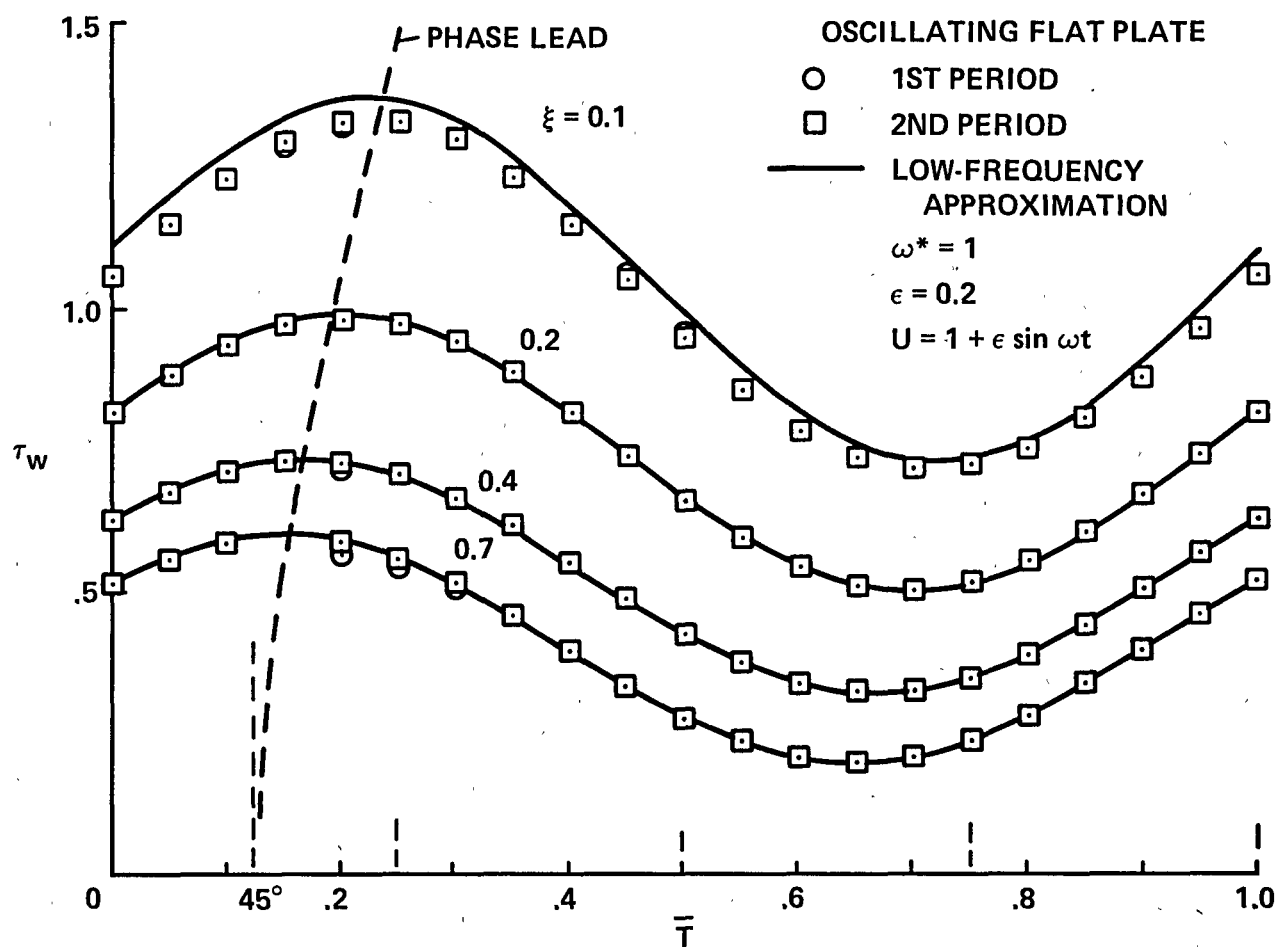
Figure 2.- Finite difference grid.

13

Figure 3.- Development of wall shear stress with respect to time at low frequency $(\omega^* = 1, \ \varepsilon = 0.2)$.
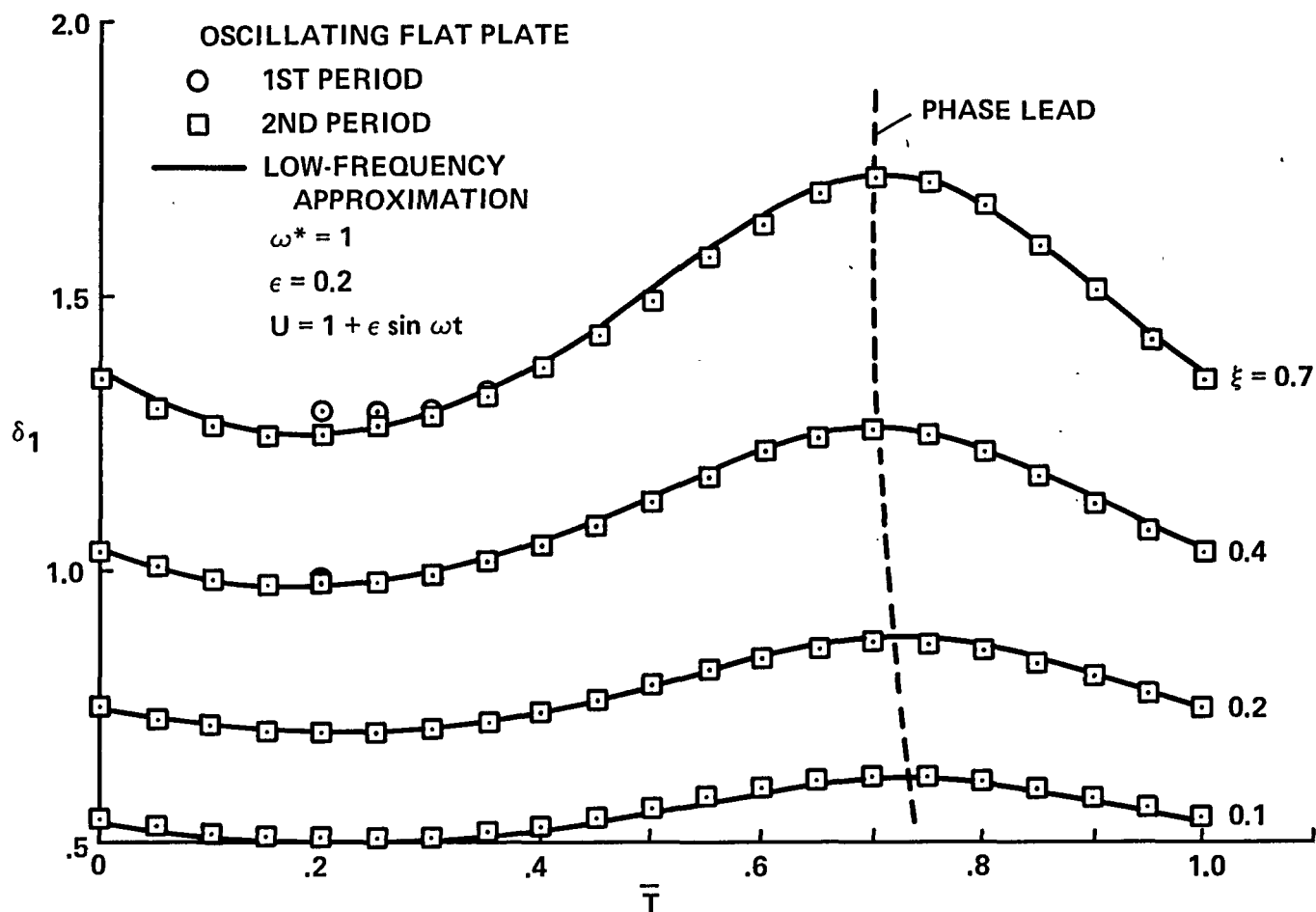
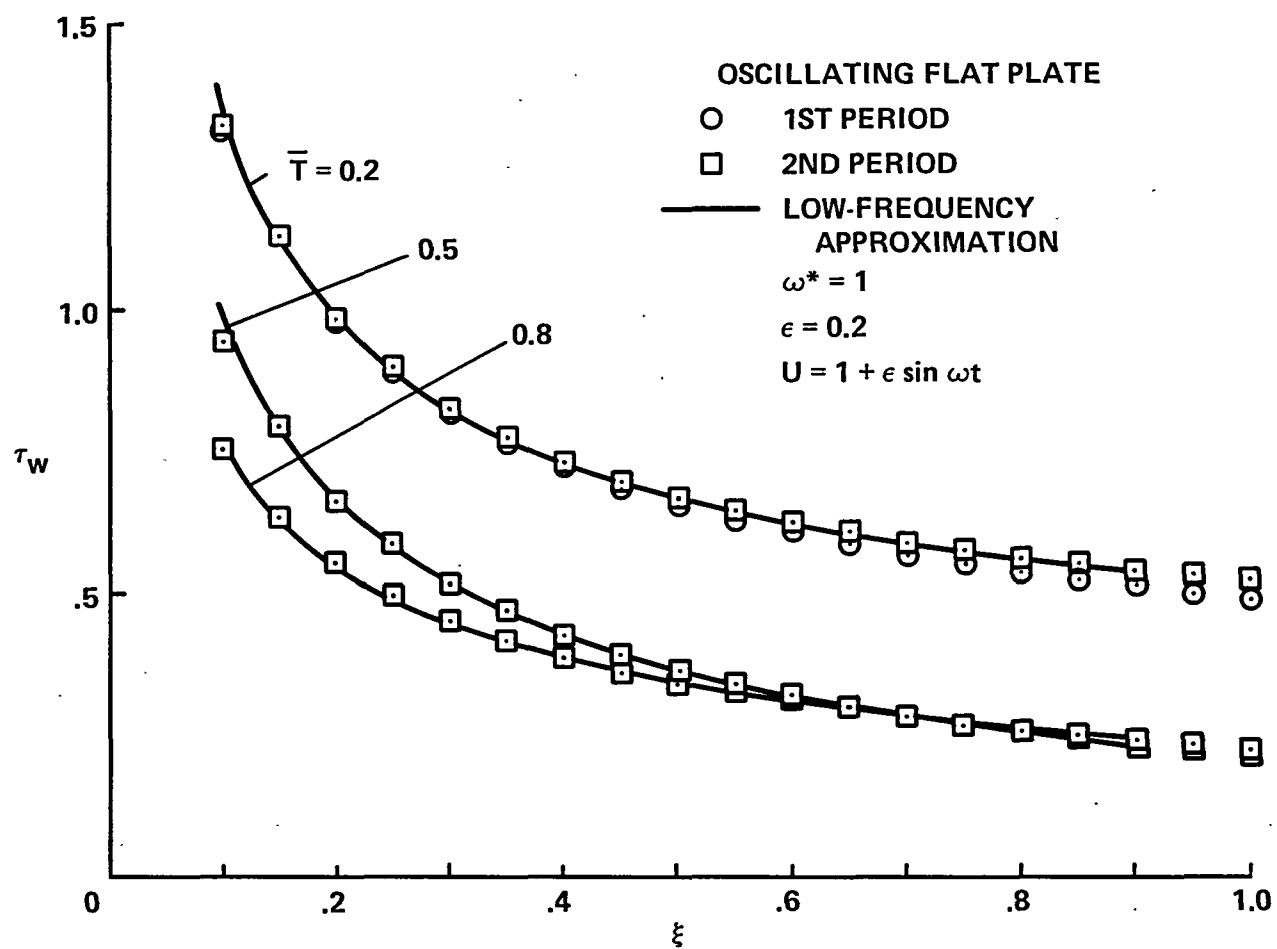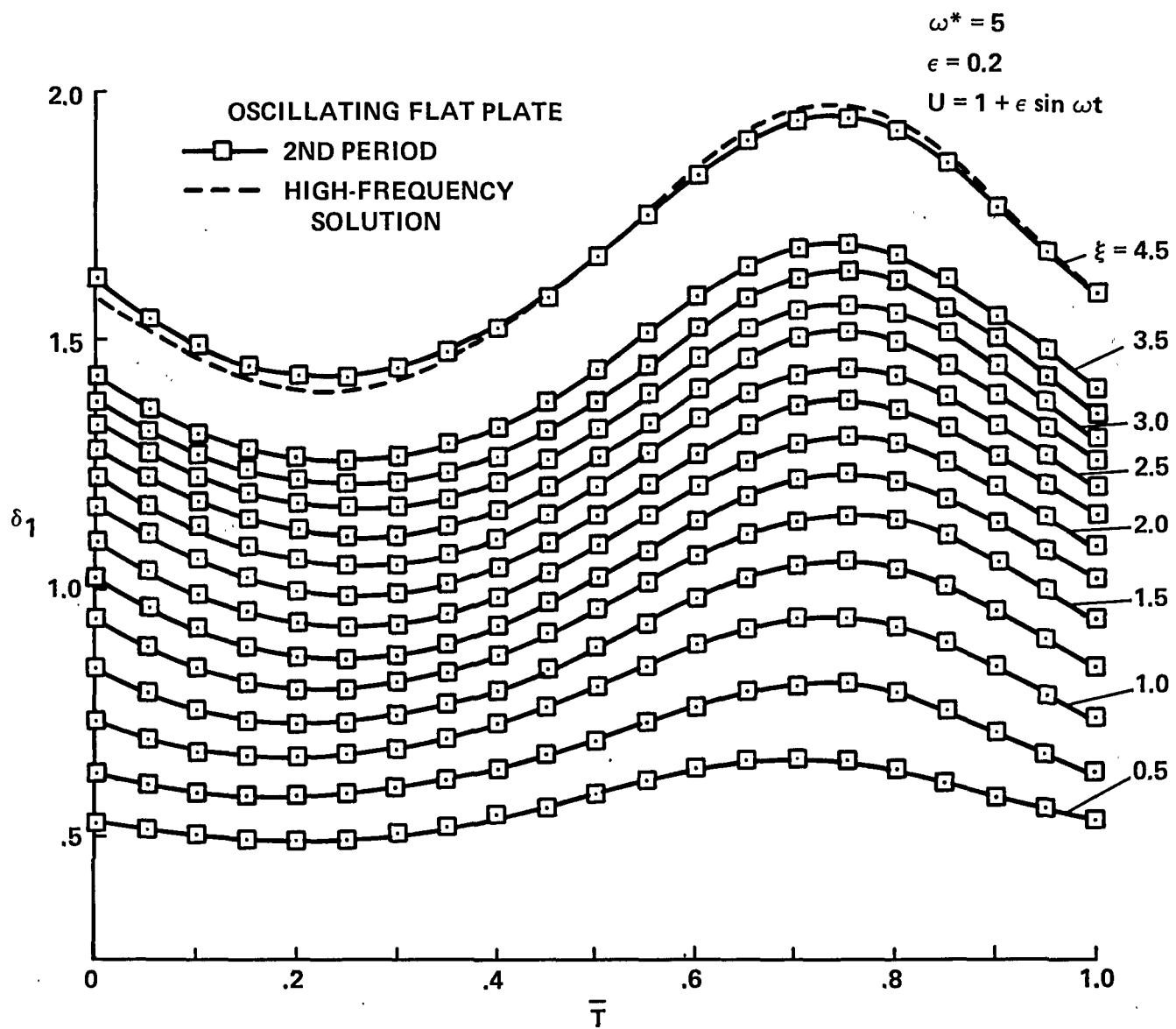Figure 4.- Development of boundary layer displacement thickness with respect to time at low frequency ($\omega^* = 1$, $\varepsilon = 0.2$).

Figure 5.– Development of wall shear stress with respect to x (ω* = 1, ϵ = 0.2).
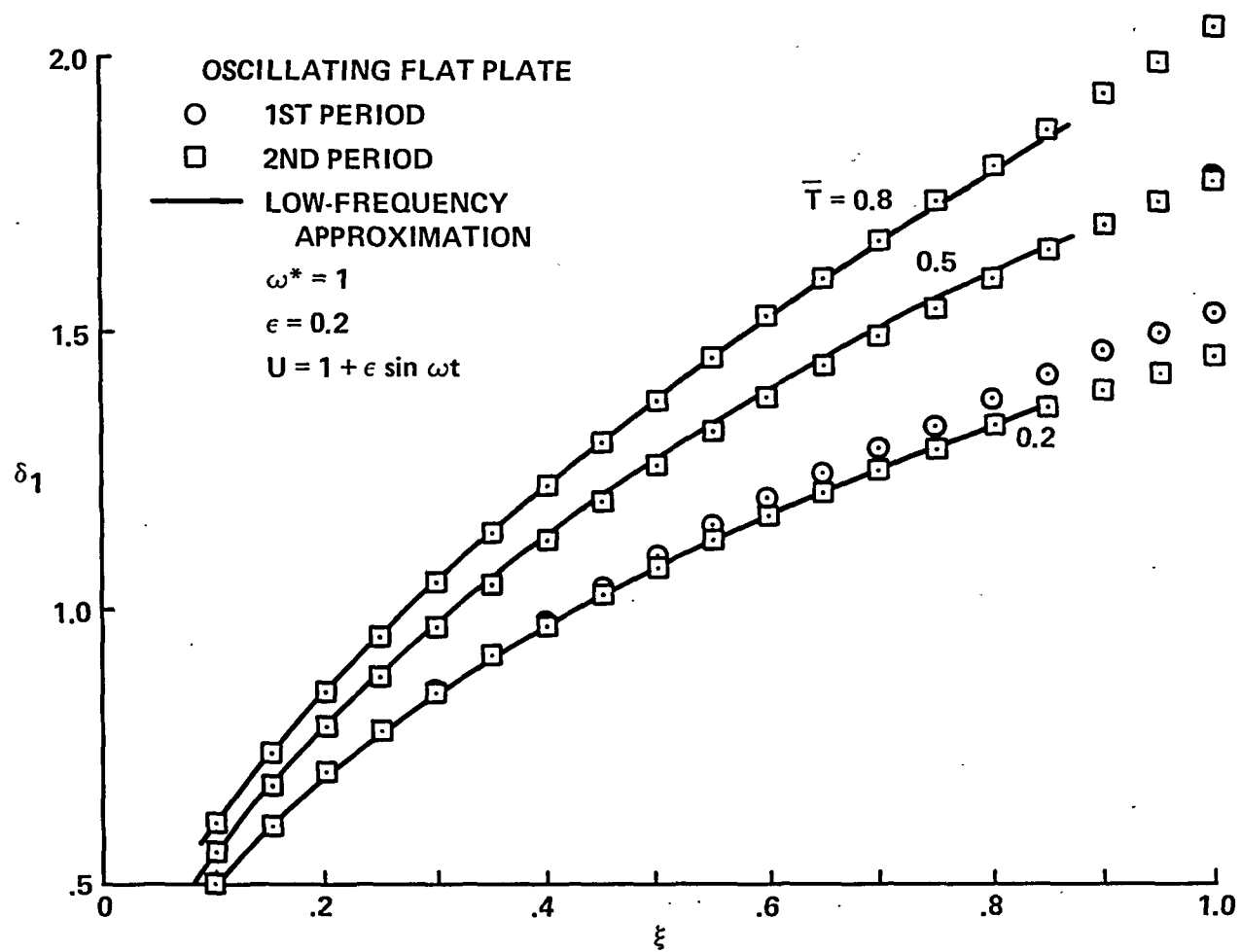
Figure 6.- Development of boundary layer displacement thickness with respect to x
$(\omega^* = 1, \ \varepsilon = 0.2)$.
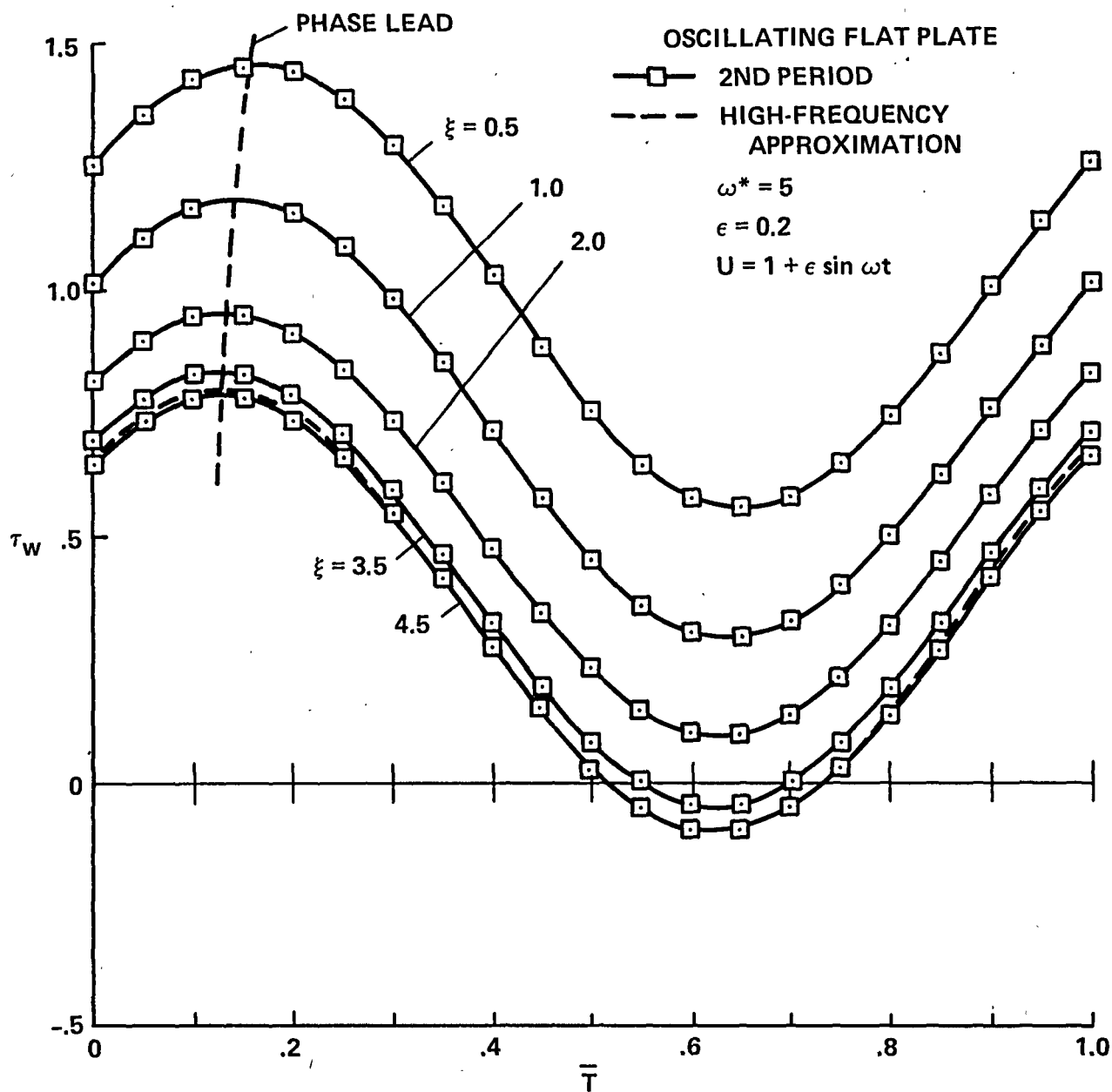
Figure 7.- Wall shear stress with respect to time at high frequency ($\omega^* = 5$, $\varepsilon = 0.2$).

18

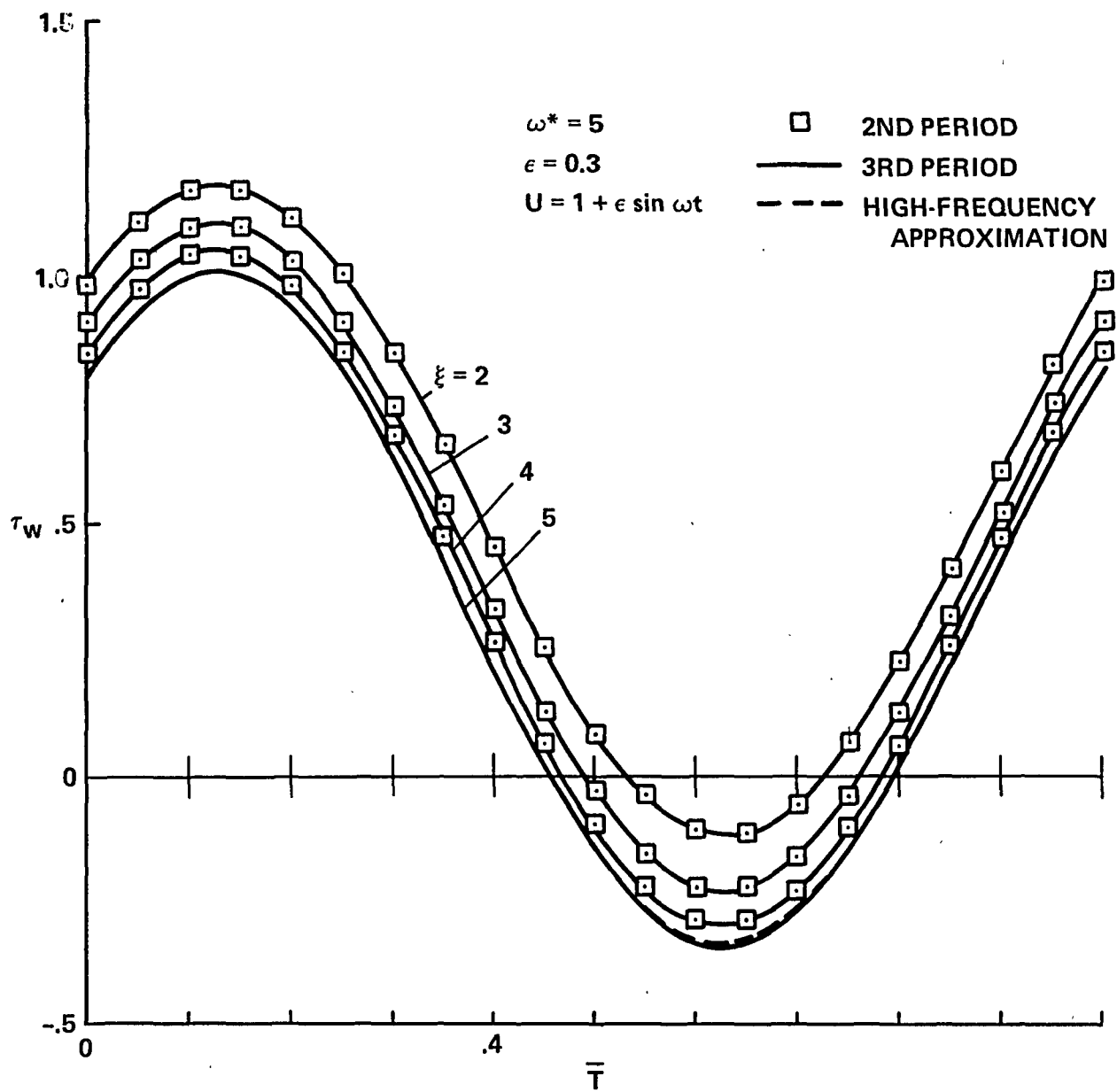Figure 8.- Boundary layer displacement thickness with respect to time at high frequency (ω* = 5, ε = 0.2).

Figure 9.- Wall shear stress with respect to time for $\omega^* = 5$, $\varepsilon = 0.3$.
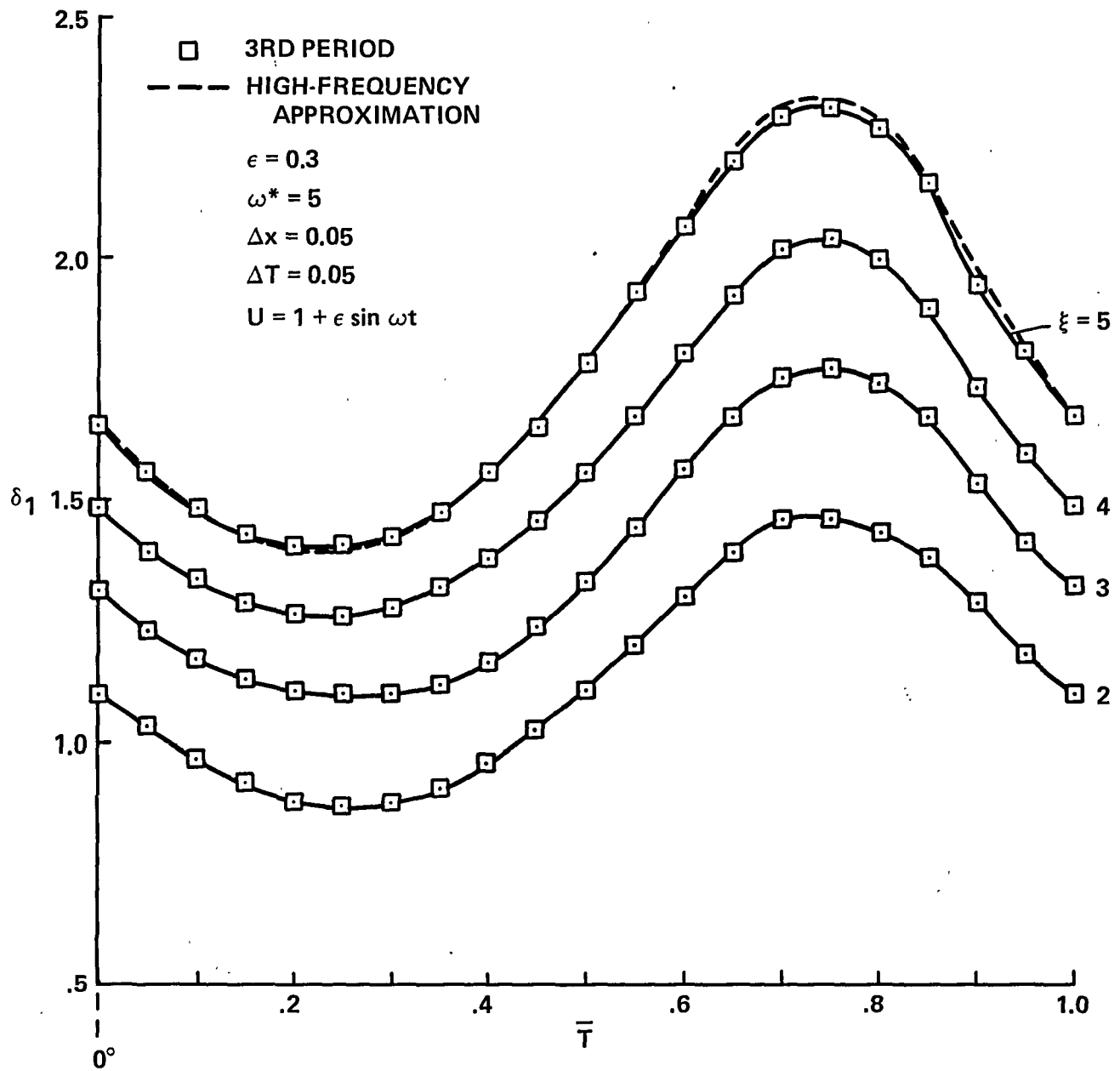
20

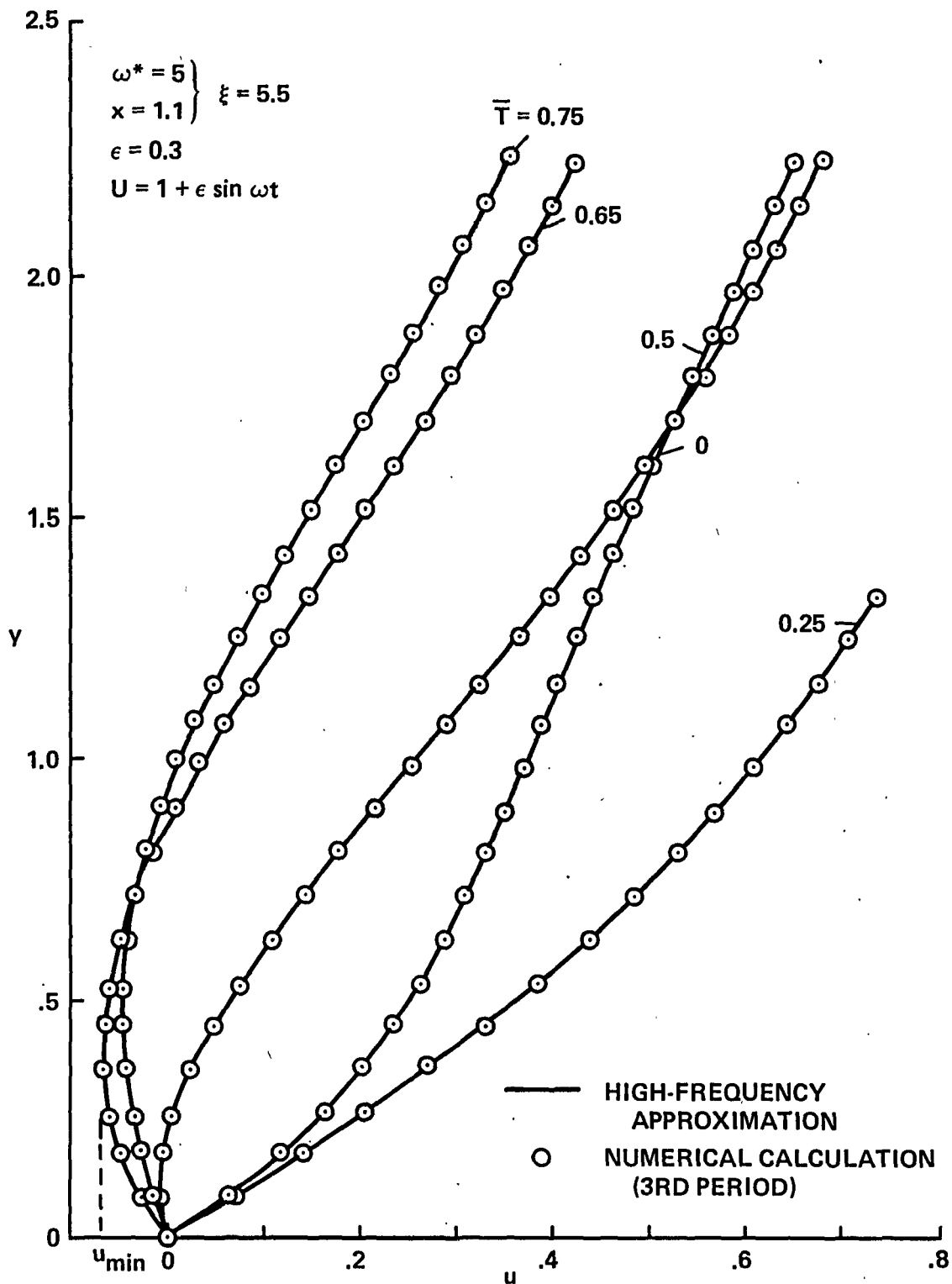Figure 10.- Boundary layer displacement thickness with respect to time for $\omega^* = 5$, $\varepsilon = 0.3$.

Figure 11.- Boundary layer profiles for $\omega^* \doteq 5$, x = 1.1 at various time levels.
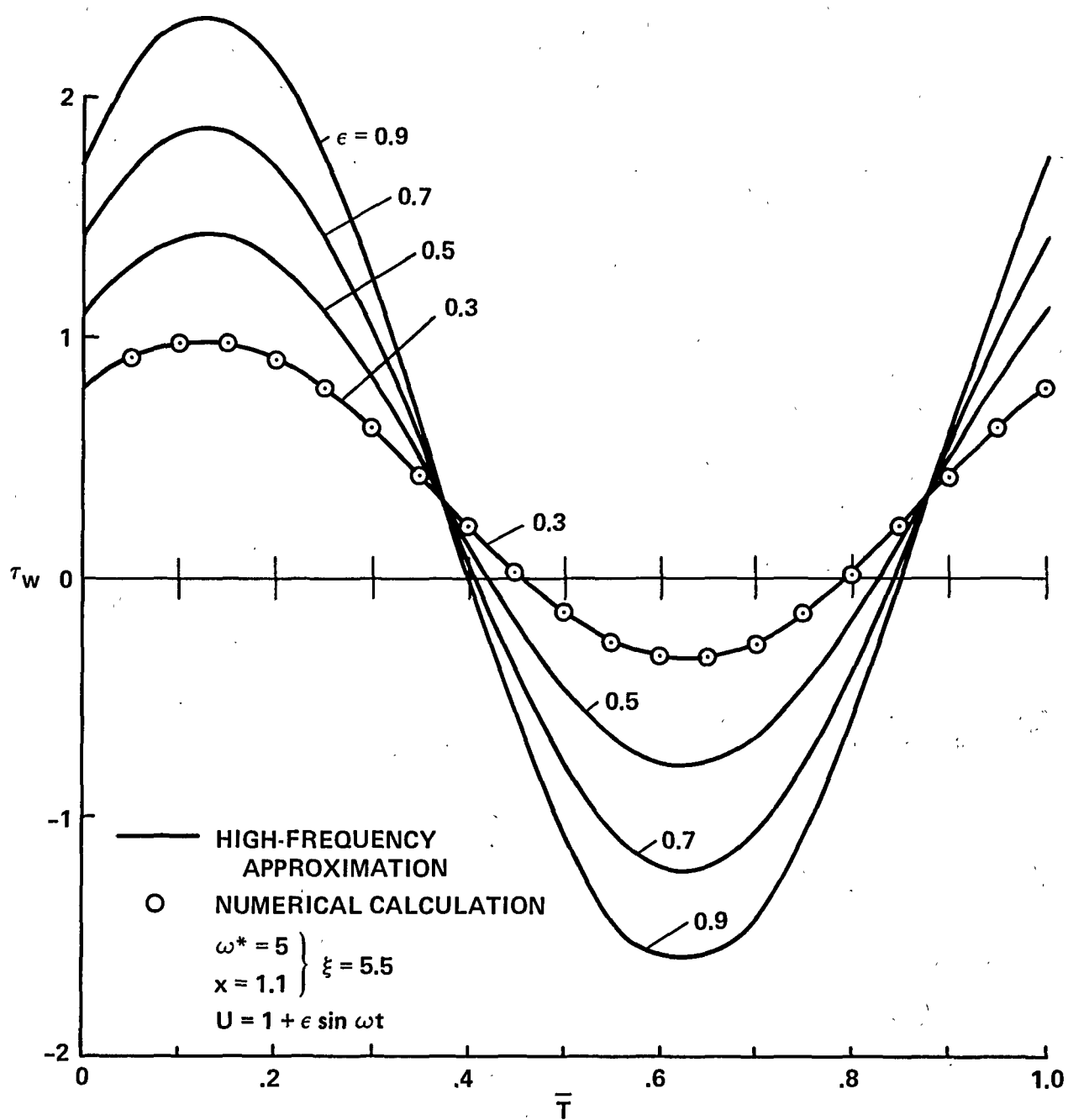
Figure 12.- Influence of oscillation amplitude on wall shear stress ($\omega^* = 5$, x = 1.1).
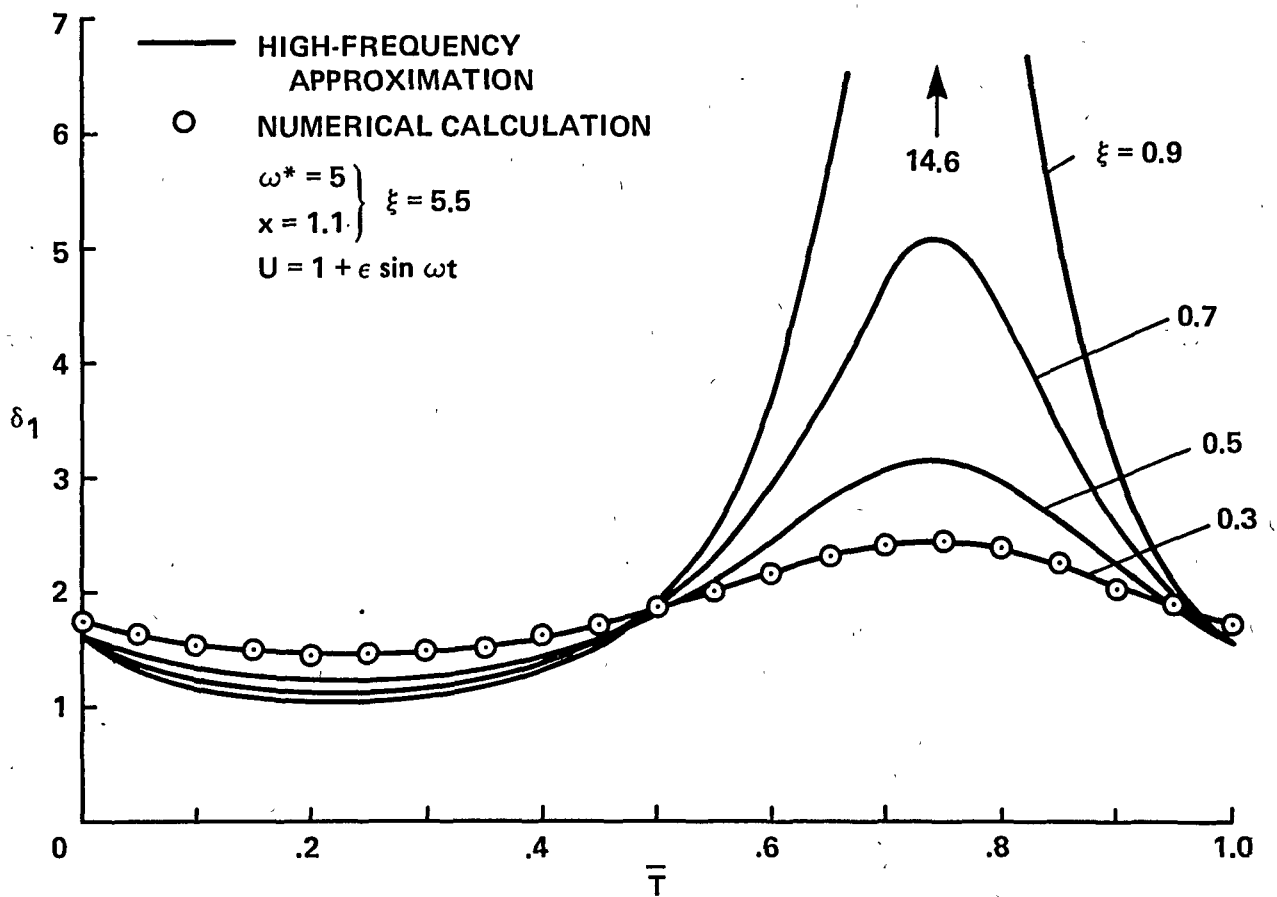
23

Figure 13.- Influence of oscillation amplitude on boundary layer displacement thickness ($\omega^* = 5$, $x = 1.1$).

1. Report No. NASA TM-84319	2. Government Accession No.	3. Recipient's Catalog No.
4. Title and Subtitle UNSTEADY LAMINAR BOUNDARY LAYER CALCULATIONS ON OSCILLATING CONFIGURATIONS INCLUDING BACKFLOW. PART I: FLAT PLATE, OSCILLATING IN ITS OWN PLANE		5. Report Date March 1983
		6. Performing Organization Code
7. Author(s) W. Geissler		8. Performing Organization Report No. A-9211
		10. Work Unit No. T-64654
9. Performing Organization Name and Address NASA Ames Research Center Moffett Field, Calif. 94035		11. Contract or Grant No.
		13. Type of Report and Period Covered Technical Memorandum
12. Sponsoring Agency Name and Address National Aeronautics and Space Administration Washington, D.C. 20546		14. Sponsoring Agency Code 505-31-01

15. Supplementary Notes

Point of Contact: W. Geissler, Ames Research Center, MS 227-8, Moffett Field, CA 94035. (415) 965-6265 or FTS 448-6265.

16. Abstract

A finite difference method has been developed to calculate the unsteady boundary layer over an oscillating flat plate. Low- and high-frequency approximations were used for comparison with numerical results. Special emphasis was placed on the behavior of the flow and on the numerical calculation procedure as soon as reversed flow has occurred over part of the oscillation cycle. The numerical method displayed neither problems nor singular behavior at the beginning of or within the reversed flow region. Calculations, however, came to a limit where the back-flow region reached the plate's leading edge in the case of high oscillation amplitudes. It is assumed that this limit is caused by the special behavior of the flow at the plate's leading edge where the boundary layer equations are not valid.

17. Key Words (Suggested by Author(s)) Unsteady viscous flow Oscillating flat plate	18. Distribution Statement Unlimited Subject Category - 02

19. Security Classif. (of this report) Unclassified	20. Security Classif. (of this page) Unclassified	21. No. of Pages 29	22. Price* A03